ACCSCIENCE PUBLISHING

International Journal of Bioprinting

RESEARCH ARTICLE

Parametric computational modeling of melt electrowritten scaffolds: Predicting the cellular micromechanical environment for gradient tissue engineering in rotator cuff repair

Supplementary File

Introduction

To characterize the gradient behavior observed in the Arc-S, parametric, finite element analysis (FEA) models of the scaffold were generated with varying radius of curvature (R), fiber diameter (FD), and fiber spacing (FS) (**Figure 1C** within the main text). The models generated were meshed with linear beam (B21) elements, fully converged, and fully validated against experimental data that mimicked the boundary and loading conditions present in benchtop testing.

To quantify the graded mechanics of each scaffold geometry, a nondimensional parameter, the strain gradient factor (SGF) was calculated by taking the ratio between the strain in the obtuse region and the strain in the acute region in each model. In total, $N = 810$ combinations of scaffold geometries were simulated using FEA to inform how print parameters alter the gradient of mechanical properties present in the architecture of the scaffold. The SGF was driven primarily by R of the scaffold with some dependence on the FD, depending on the R of each scaffold.

Figures S1–S8 in **Supplemental 1** are representative 3D surface plots of the SGF calculated from FEA predications in the fiber model at FS = 200, 300, 350, 400, 450, 500, 550, and 600 μm. All data presented below were discussed in the results and utilized in the Spearman's correlation coefficient analysis.

To predict the multitissue healing functionality of the Arc-S, additional parametric models of the unit cell (UC) in four regions of each scaffold geometry were created. These models were meshed with 2D plane stress linear elements (CPS3), as a linear elastic material with $E = 50$ kPa, $= 0.3$, and loaded with displacements that correspond to the regional displacement in each scaffold. Four regions on each scaffold were named the "middle acute," "outer acute," "middle obtuse," and "outer obtuse." After analysis, UC element hydrostatic pressure and strains were plotted against a tissue healing window based on previously published *in vitro* data that promoted bone and tendon healing to quantify the percentage of elements that are within the healing boundary. $N = 3240$ simulations were run to predict the potential bone and tendon healing of the scaffold. Additionally, UC element eigenvectors were fitted with a von Mises distribution to predict how concentrated the alignment of the principal strain would be, with the goal that the scaffold geometry would drive cellular alignment in the tendon region to mimic native tissue.

Figures S9–S16 in **Supplemental 2** are representative 3D surface plots of the tissue healing window percentages calculated from FEA predictions of FS = 200, 300, 350, 400, 450, 500, 550, and 600 μm. All data presented below were discussed in the results and utilized in the Spearman's correlation coefficient analysis.

Figures S17–S24 in **Supplemental 3** are representative 3D surface plots of the tissue healing window percentages calculated from FEA predictions of FS = 200, 250, 300, 350, 400, 450, 500, and 550 μm. All data presented below were discussed in the results and utilized in the Spearman's correlation coefficient analysis.

Supplemental 1

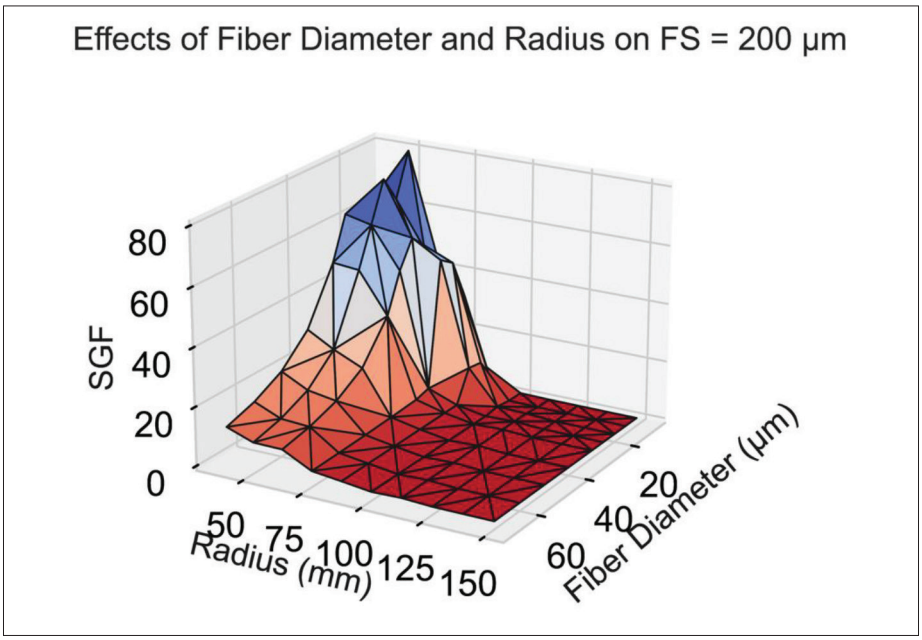

Figure S1. Representative 3D surface plot of FEA predictions (N = 90) with strain gradient factor (SGF) plotted against fiber diameter (FD) and radius (R) at the same fiber spacing (RS) = 200 µm. Peak SGF = 83 was reached at R = 38 mm and FD = 30 µm, approaching the gradient present in human rotator cuff. Spearman's correlation coefficients for R, D, and FS were −0.93, −0.068, and −0.048, respectively.

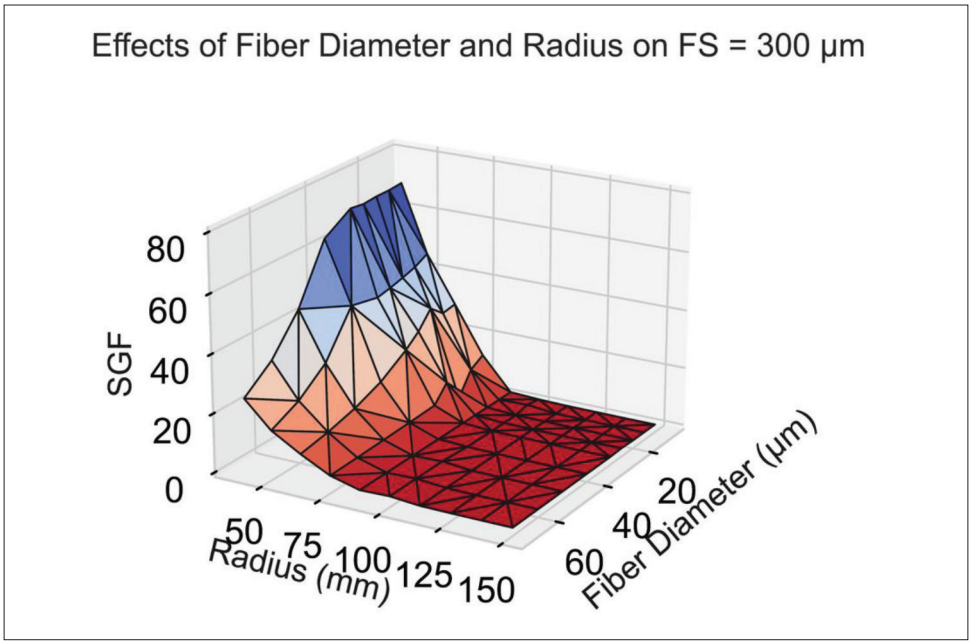

Figure S2. Representative 3D surface plot of FEA predictions (N = 90) with strain gradient factor (SGF) plotted against fiber diameter (FD) and radius (R) at the same fiber spacing (FS) = 300 µm. Peak SGF = 83 was reached at R = 38 mm and FD = 30 µm, approaching the gradient present in human rotator cuff. Spearman's correlation coefficients for R, D, and FS were −0.93, −0.068, and −0.048, respectively.

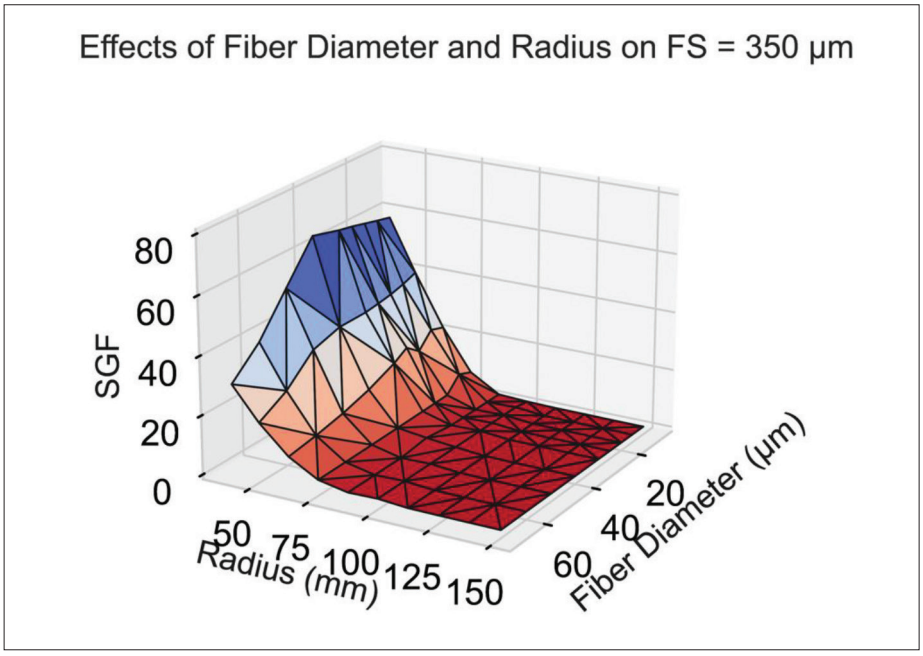

Figure S3. Representative 3D surface plot of FEA predictions (N = 90) with strain gradient factor (SGF) plotted against fiber diameter (FD) and radius (R) at the same fiber spacing (FS) = 350 μm. Peak SGF = 83 was reached at R = 38 mm and FD = 30 μm, approaching the gradient present in human rotator cuff. Spearman's correlation coefficients for R, D, and FS were −0.93, −0.068, and −0.048, respectively.

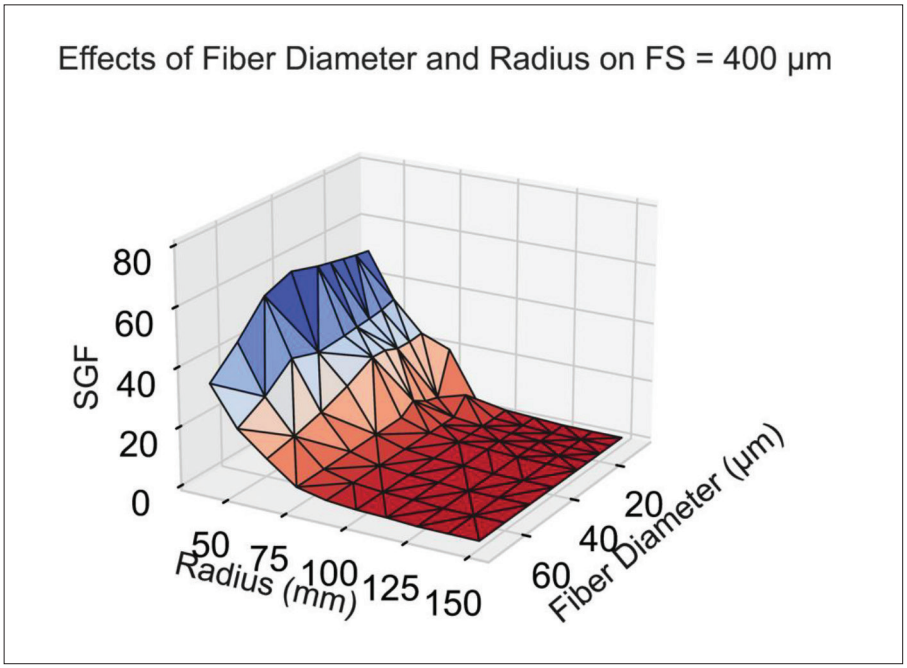

Figure S4. Representative 3D surface plot of FEA predictions (N = 90) with strain gradient factor (SGF) plotted against fiber diameter (FD) and radius (R) at the same fiber spacing (FS) = 400 μm. Peak SGF = 83 was reached at R = 38 mm and FD = 30 μm, approaching the gradient present in human rotator cuff. Spearman's correlation coefficients for R, D, and FS were −0.93, −0.068, and −0.048, respectively.

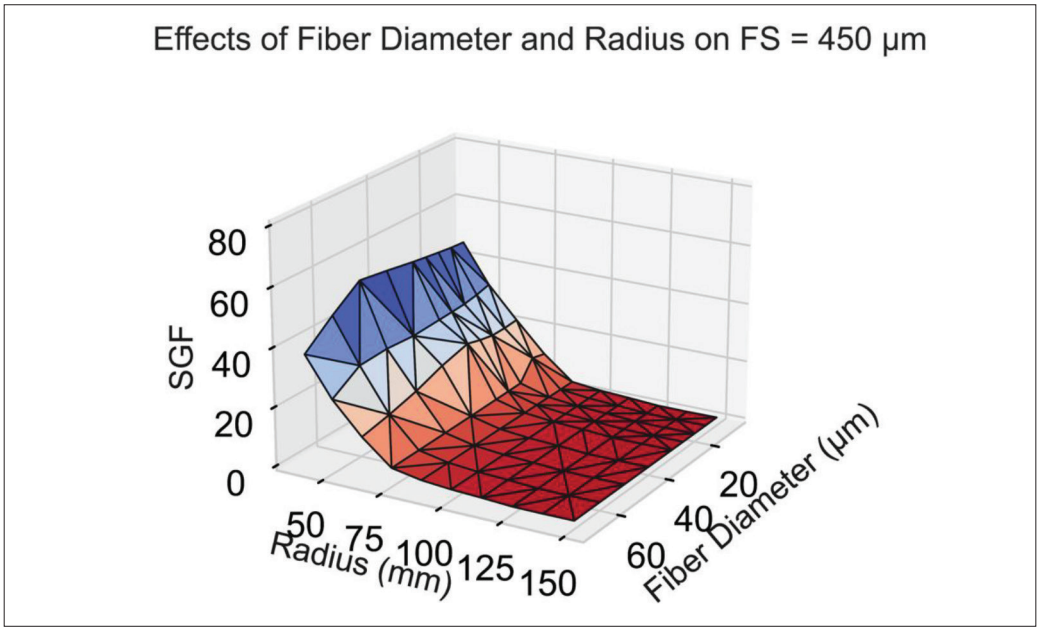

Figure S5. Representative 3D surface plot of FEA predictions ($N = 90$) with strain gradient factor (SGF) plotted against fiber diameter (FD) and radius (R) at the same fiber spacing (FS) = 450 μm. Peak SGF = 83 was reached at R = 38 mm and FD = 30 μm, approaching the gradient present in human rotator cuff. Spearman's correlation coefficients for R, D, and FS were −0.93, −0.068, and −0.048, respectively.

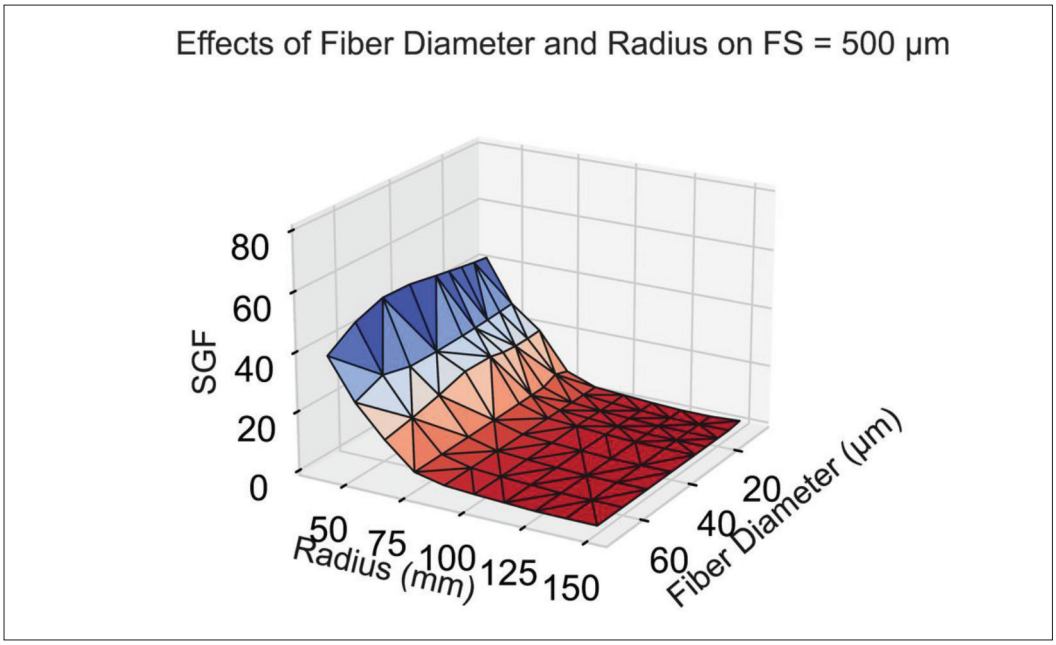

Figure S6. Representative 3D surface plot of FEA predictions ($N = 90$) with strain gradient factor (SGF) plotted against fiber diameter (FD) and radius (R) at the same fiber spacing (FS) = 500 μm. Peak SGF = 83 was reached at R = 38 mm and FD = 30 μm, approaching the gradient present in human rotator cuff. Spearman's correlation coefficients for R, D, and FS were −0.93, −0.068, and −0.048, respectively.

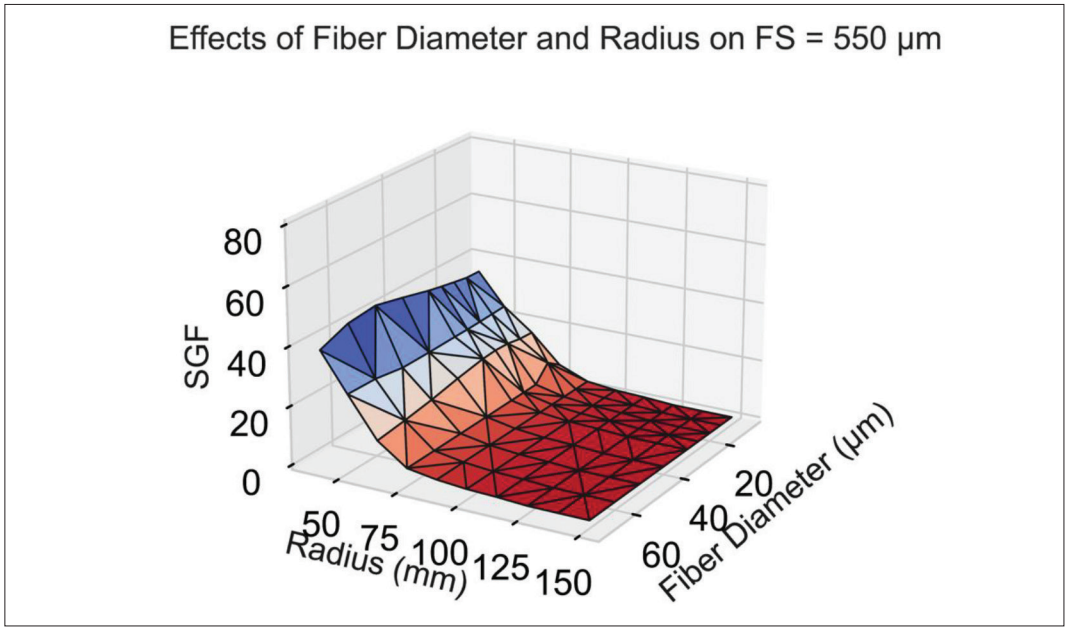

Figure S7. Representative 3D surface plot of FEA predictions ($N = 90$) with strain gradient factor (SGF) plotted against fiber diameter (FD) and radius (R) at the same fiber spacing (FS) = 550 µm. Peak SGF = 83 was reached at $R = 38$ mm and FD = 30 µm, approaching the gradient present in human rotator cuff. Spearman's correlation coefficients for R, D, and FS were −0.93, −0.068, and −0.048, respectively.

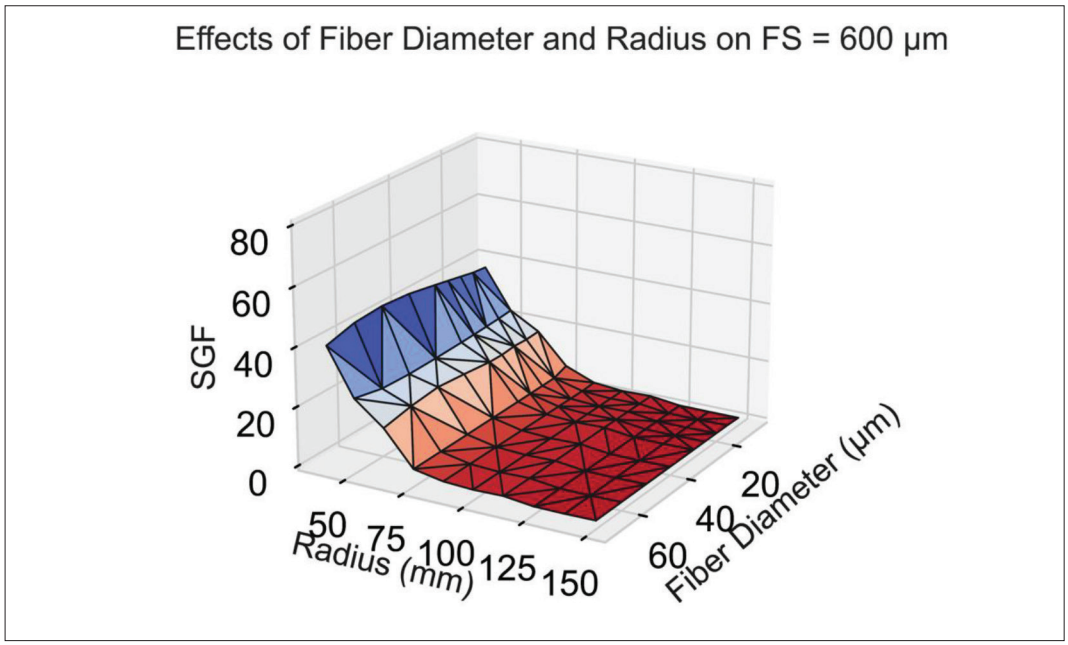

Figure S8. Representative 3D surface plot of FEA predictions ($N = 90$) with strain gradient factor (SGF) plotted against fiber diameter (FD) and radius (R) at the same fiber spacing (FS) = 600 µm. Peak SGF = 83 was reached at $R = 38$ mm and FD = 30 µm, approaching the gradient present in human rotator cuff. Spearman's correlation coefficients for R, D, and FS were −0.93, −0.068, and −0.048, respectively.

Supplemental 2

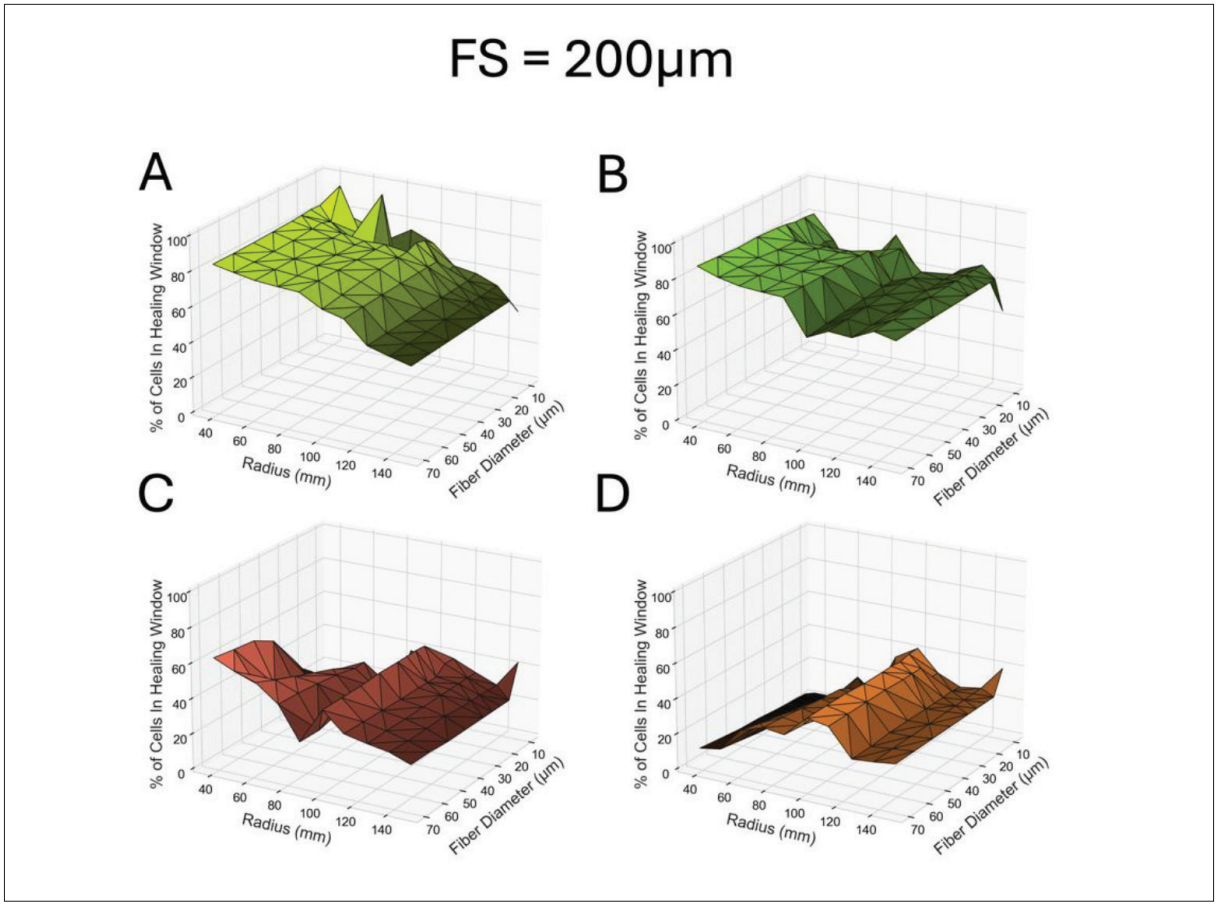

Figure S9. Representative plots of tissue healing window percentages in the outer acute region (A), middle acute region (B), outer obtuse region (C), and middle obtuse region (D) for a single fiber spacing (FS) = 200 μm. Both acute regions trended lower as radius (*R*) increased, with little difference in fiber diameter (FD). Spearman's correlation coefficients for all *R*, FD, and FS in the outer acute region were −0.81, 0.081, and −0.31, respectively. Spearman's correlation coefficients for all *R*, FD, and FS in the middle acute region were −0.34, 0.21, and −0.44, respectively. Both obtuse regions trended lower as *R* increased, with little difference in FD. Spearman's correlation coefficients for all *R*, FD, and FS in the outer acute region were 0.2, 0.32, and −0.082, respectively. Spearman's correlation coefficients for all *R*, FD, and FS in the middle obtuse region were 0.66, 0.12, and −0.017, respectively.

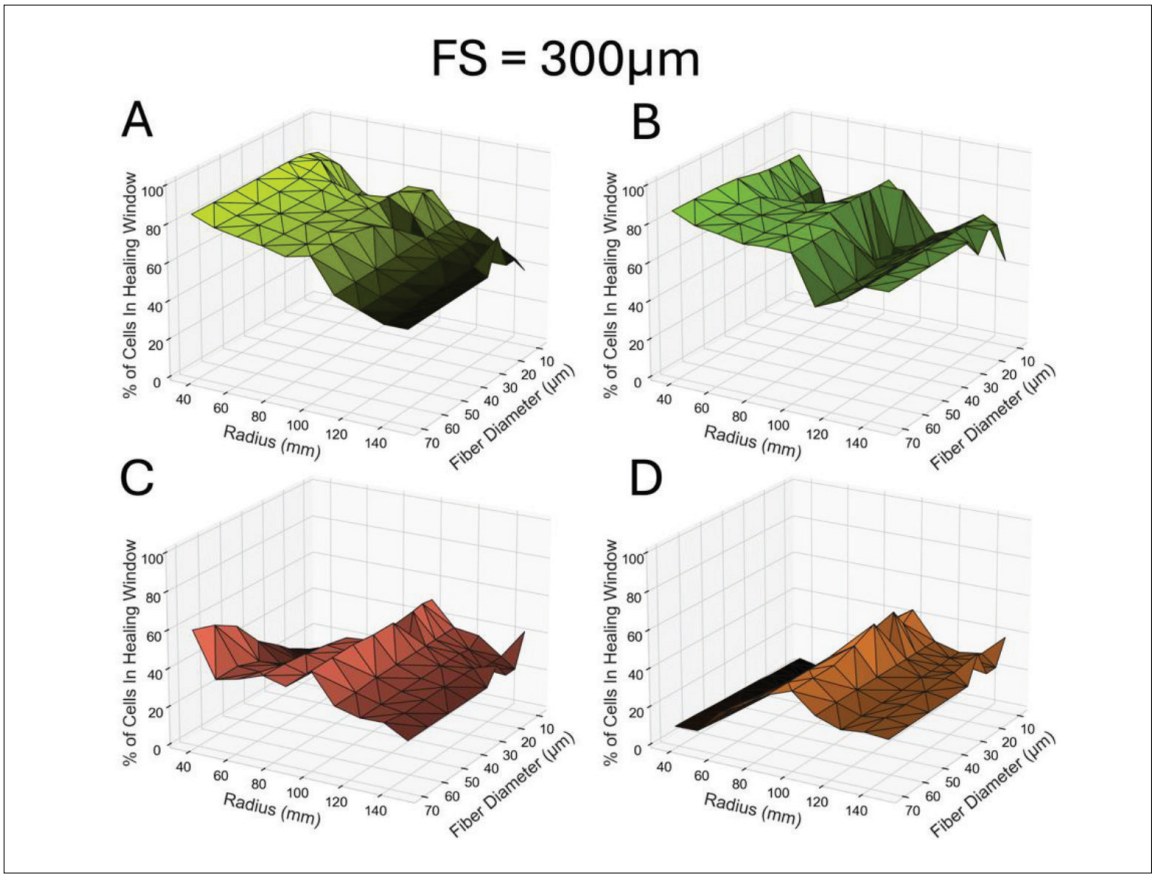

Figure S10. Representative plots of tissue healing window percentages in the outer acute region (A), middle acute region (B), outer obtuse region (C), and middle obtuse region (D) for a single fiber spacing (FS) = 300 μm. Both acute regions trended lower as radius (*R*) increased, with little difference in fiber diameter (FD). Spearman's correlation coefficients for all *R*, FD, and FS in the outer acute region −0.81, 0.081, and −0.31, respectively. Spearman's correlation coefficients for all *R*, FD, and FS in the middle acute region were −0.34, 0.21, and −0.44, respectively. Both obtuse regions trended lower as *R* increased, with little difference in FD. Spearman's correlation coefficients for all *R*, FD, and FS in the outer acute region were 0.2, 0.32, and −0.082, respectively. Spearman's correlation coefficients for all *R*, FD, and FS in the middle obtuse region were 0.66, 0.12, and −0.017, respectively.

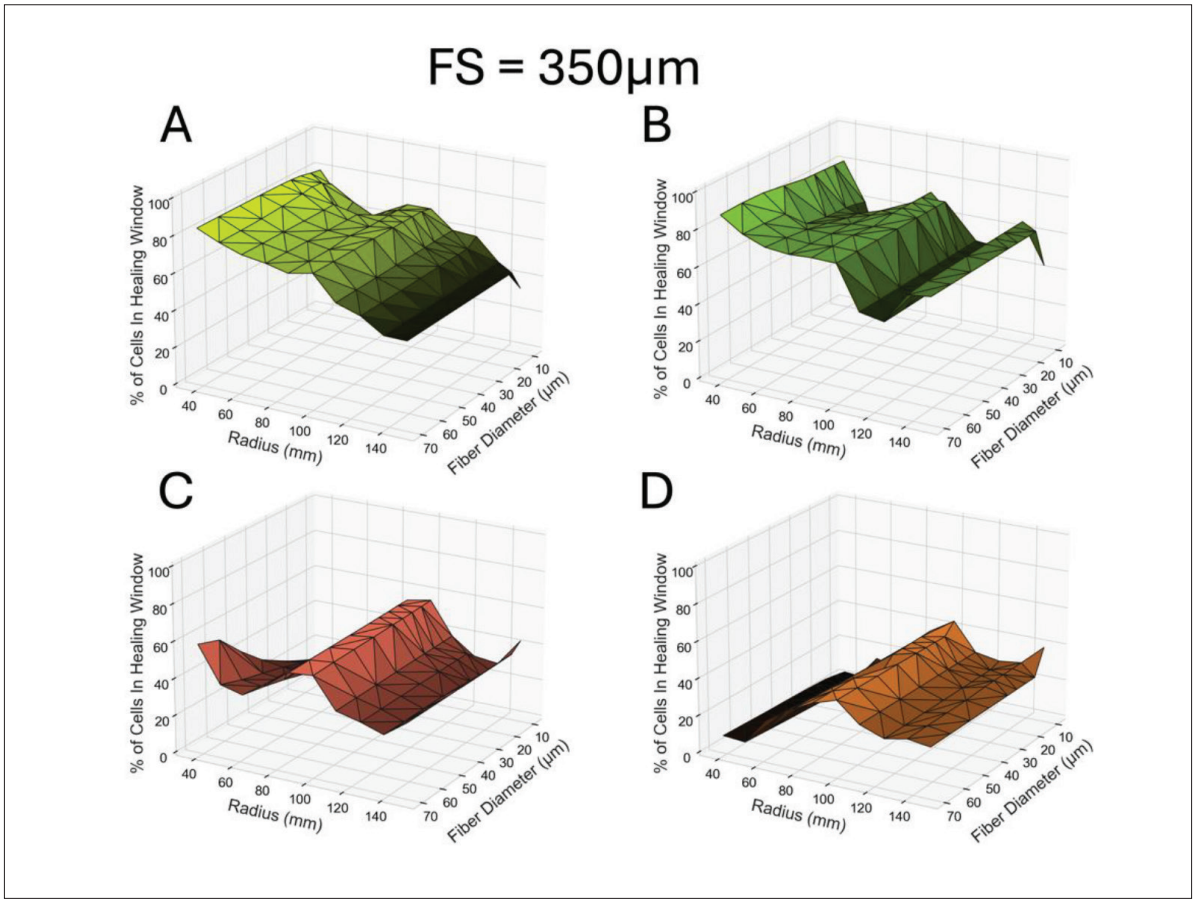

Figure S11. Representative plots of tissue healing window percentages in the outer acute region (A), middle acute region (B), outer obtuse region (C), and middle obtuse region (D) for a single fiber spacing (FS) = 350 μm. Both acute regions trended lower as radius (*R*) increased, with little difference in fiber diameter (FD). Spearman's correlation coefficients for all *R*, *D*, and FS in the outer acute region were −0.81, 0.081, and −0.31, respectively. Spearman's correlation coefficients for all *R*, FD, and FS in the middle acute region were −0.34, 0.21, and −0.44, respectively. Both obtuse regions trended lower as *R* increased, with little difference in FD. Spearman's correlation coefficients for all *R*, FD, and FS in the outer acute region were 0.2, 0.32, and −0.082, respectively. Spearman's correlation coefficients for all *R*, FD, and FS in the middle obtuse region were 0.66, 0.12, and −0.017, respectively.

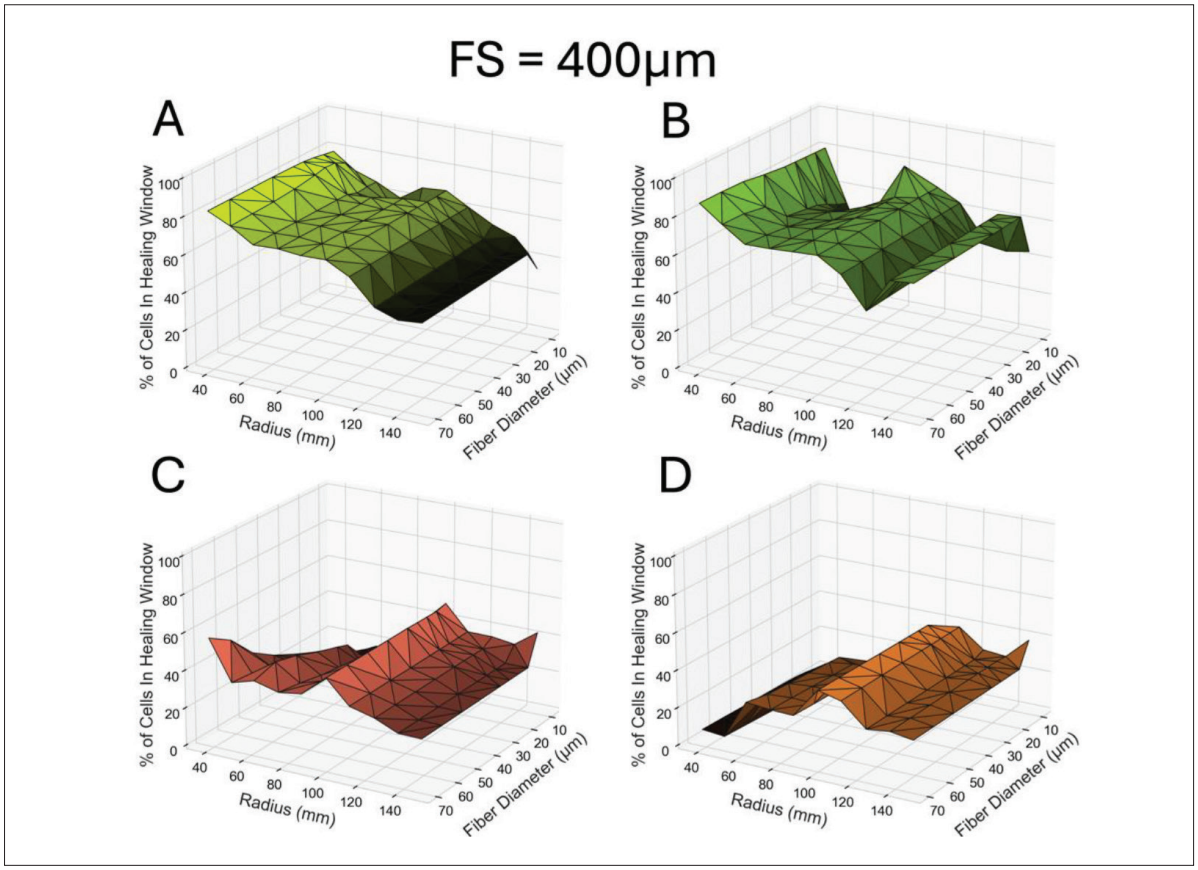

Figure S12. Representative plots of tissue healing window percentages in the outer acute region (A), middle acute region (B), outer obtuse region (C), and middle obtuse region (D) for a single fiber spacing (FS) = 400 μm. Both acute regions trended lower as radius (*R*) increased, with little difference in fiber diameter (FD). Spearman's correlation coefficients for all *R*, FD, and FS in the outer acute region were −0.81, 0.081, and −0.31, respectively. Spearman's correlation coefficients for all *R*, FD, and FS in the middle acute region were −0.34, 0.21, and −0.44, respectively. Both obtuse regions trended lower as *R* increased, with little difference in FD. Spearman's correlation coefficients for all *R*, FD, and FS in the outer acute region were 0.2, 0.32, and −0.082, respectively. Spearman's correlation coefficients for all *R*, FD, and FS in the middle obtuse region were 0.66, 0.12, and −0.017, respectively.

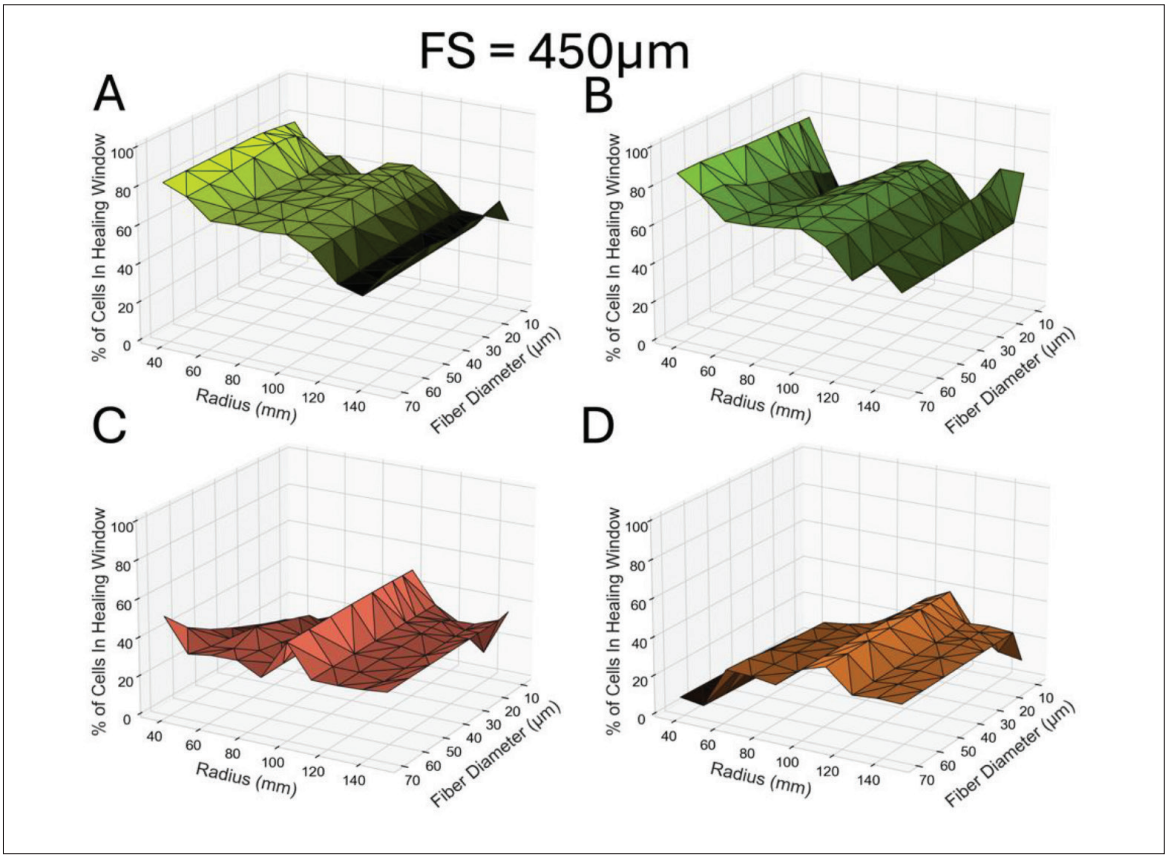

Figure S13. Representative plots of tissue healing window percentages in the outer acute region (A), middle acute region (B), outer obtuse region (C), and middle obtuse region (D) for a single fiber spacing (FS) = 450 μm. Both acute regions trended lower as radius (*R*) increased, with little difference in fiber diameter (FD). Spearman's correlation coefficients for all *R*, FD, and FS in the outer acute region were −0.81, 0.081, and −0.31, respectively. Spearman's correlation coefficients for all *R*, FD, and FS in the middle acute region were −0.34, 0.21, and −0.44, respectively. Both obtuse regions trended lower as *R* increased, with little difference in FD. Spearman's correlation coefficients for all R, FD, and FS in the outer acute region 0.2, 0.32, and −0.082, respectively. Spearman's correlation coefficients for all R, FD, and FS in the middle obtuse region were 0.66, 0.12, and −0.017, respectively.

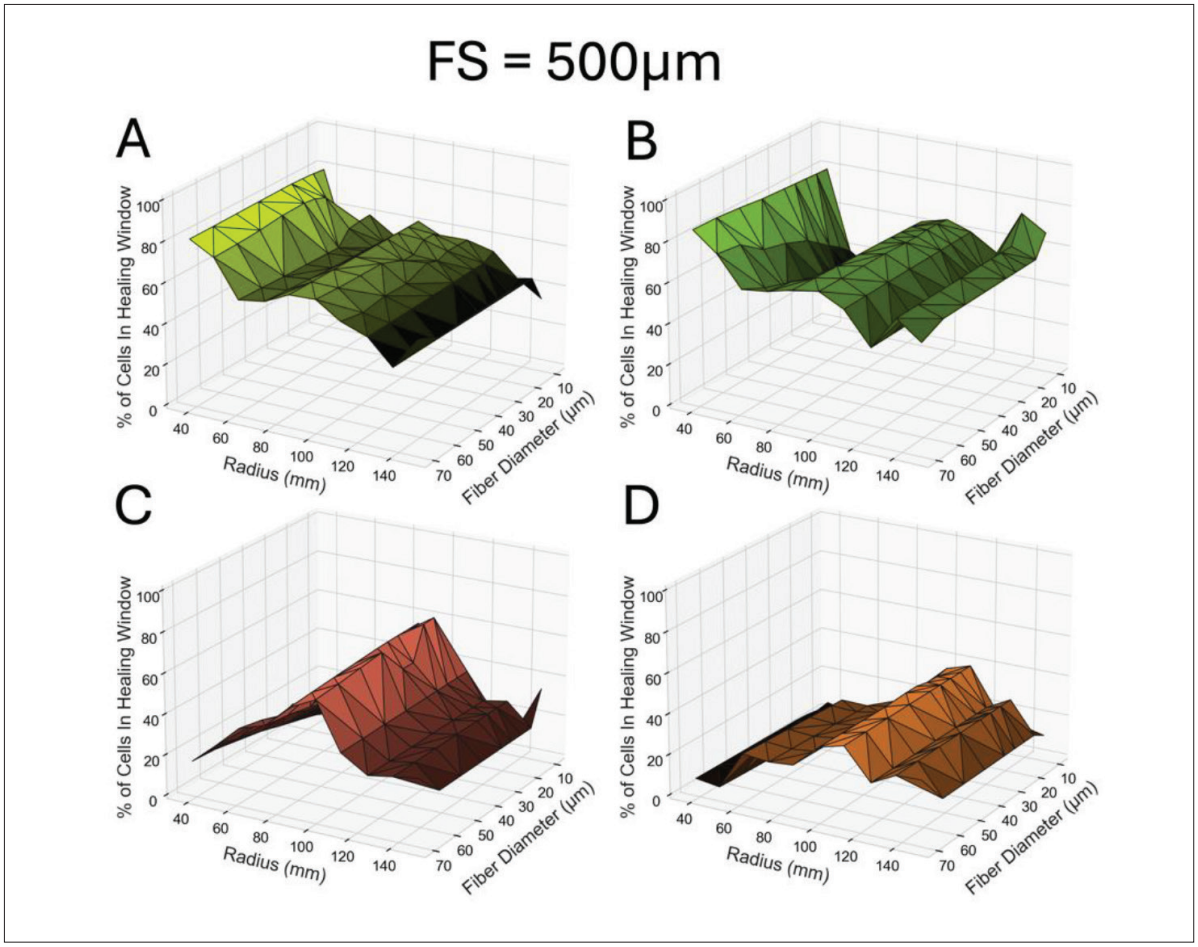

Figure S14. Representative plots of tissue healing window percentages in the outer acute region (A), middle acute region (B), outer obtuse region (C), and middle obtuse region (D) for a single fiber spacing (FS) = 500 μm. Both acute regions trended lower as radius (*R*) increased, with little difference in fiber diameter (FD). Spearman's correlation coefficients for all *R*, FD, and FS in the outer acute region were −0.81, 0.081, and −0.31, respectively. Spearman's correlation coefficients for all *R*, FD, and FS in the middle acute region were −0.34, 0.21, and −0.44, respectively. Both obtuse regions trended lower as *R* increased, with little difference in FD. Spearman's correlation coefficients for all *R*, FD, and FS in the outer acute region were 0.2, 0.32, and −0.082, respectively. Spearman's correlation coefficients for all *R*, FD, and FS in the middle obtuse region were 0.66, 0.12, and −0.017, respectively.

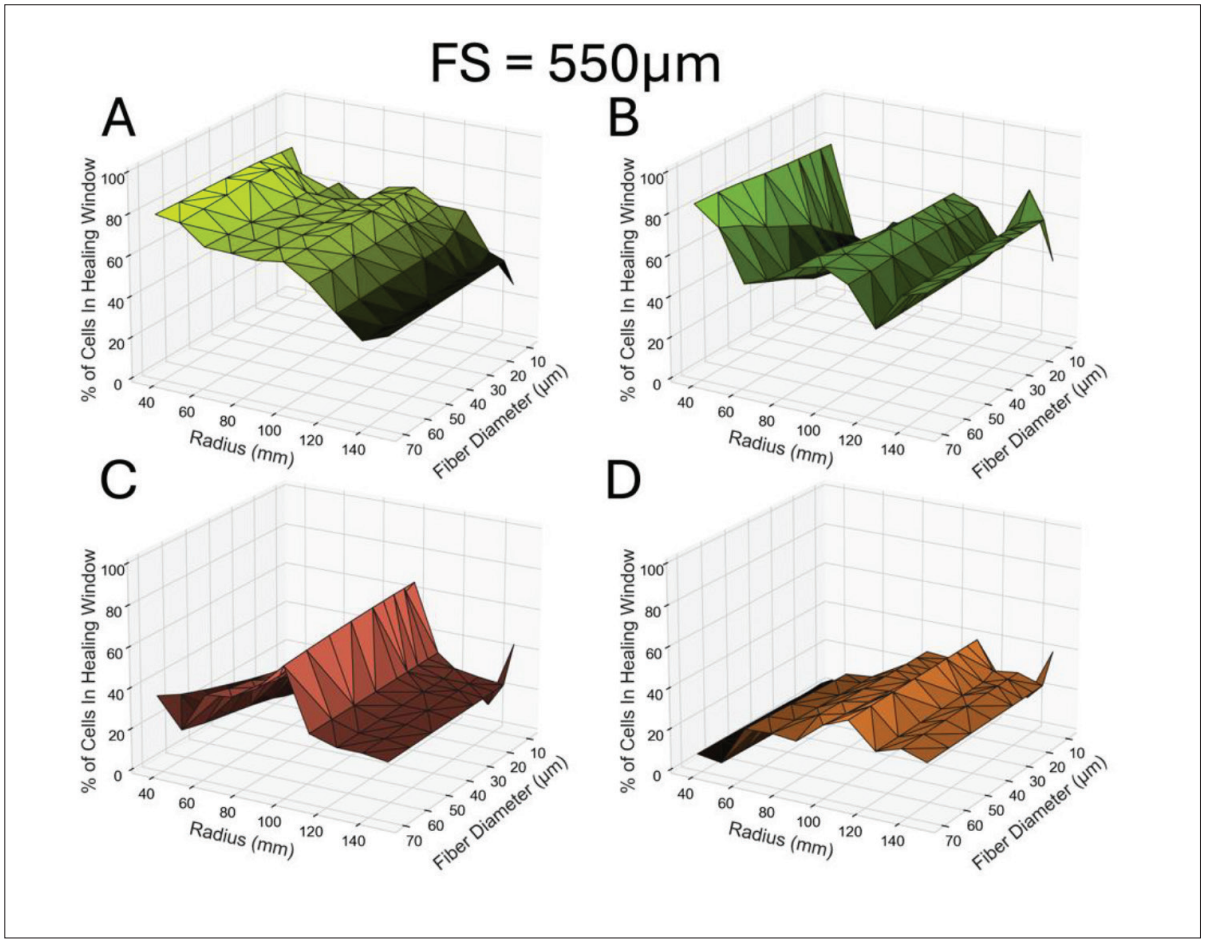

Figure S15. Representative plots of tissue healing window percentages in the outer acute region (A), middle acute region (B), outer obtuse region (C), and middle obtuse region (D) for a single fiber spacing (FS) = 550 µm. Both acute regions trended lower as radius (*R*) increased, with little difference in fiber diameter (FD). Spearman's correlation coefficients for all *R*, FD, and FS in the outer acute region were −0.81, 0.081, and −0.31, respectively. Spearman's correlation coefficients for all *R*, FD, and FS in the middle acute region were −0.34, 0.21, and −0.44, respectively. Both obtuse regions trended lower as R increased, with little difference in FD. Spearman's correlation coefficients for all *R*, FD, and FS in the outer acute region were 0.2, 0.32, and −0.082, respectively. Spearman's correlation coefficients for all *R*, FD, and FS in the middle obtuse region were 0.66, 0.12, and −0.017, respectively.

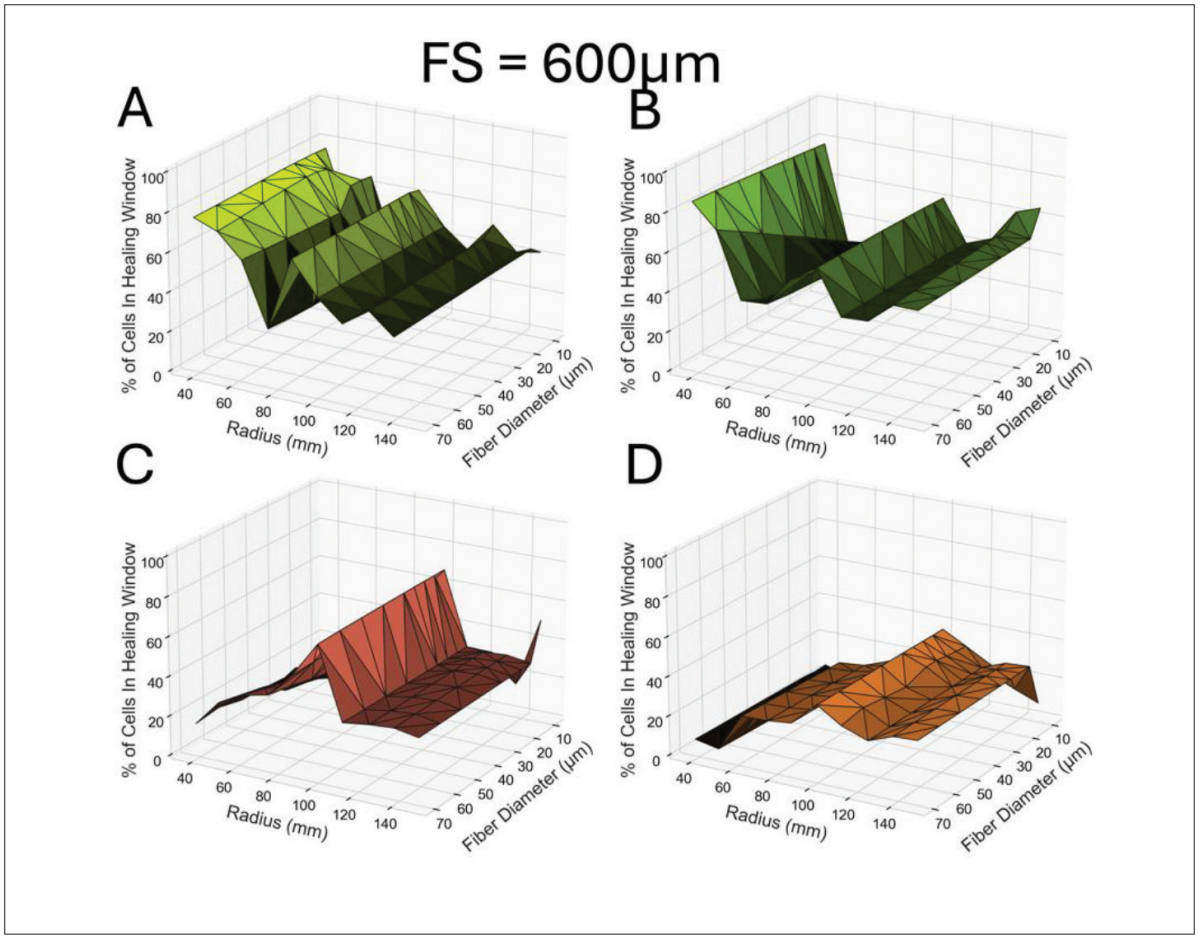

Figure S16. Representative plots of tissue healing window percentages in the outer acute region (A), middle acute region (B), outer obtuse region (C), and middle obtuse region (D) for a single fiber spacing (FS) = 600 µm. Both acute regions trended lower as radius (*R*) increased, with little difference in fiber diameter (FD). Spearman's correlation coefficients for all R, FD, and FS in the outer acute region were −0.81, 0.081, and −0.31, respectively. Spearman's correlation coefficients for all *R*, FD, and FS in the middle acute region were −0.34, 0.21, and −0.44, respectively. Both obtuse regions trended lower as R increased, with little difference in FD. Spearman's correlation coefficients for all *R*, FD, and FS in the outer acute region were 0.2, 0.32, and −0.082, respectively. Spearman's correlation coefficients for all *R*, FD, and FS in the middle obtuse region were 0.66, 0.12, and −0.017, respectively.

Supplemental 3

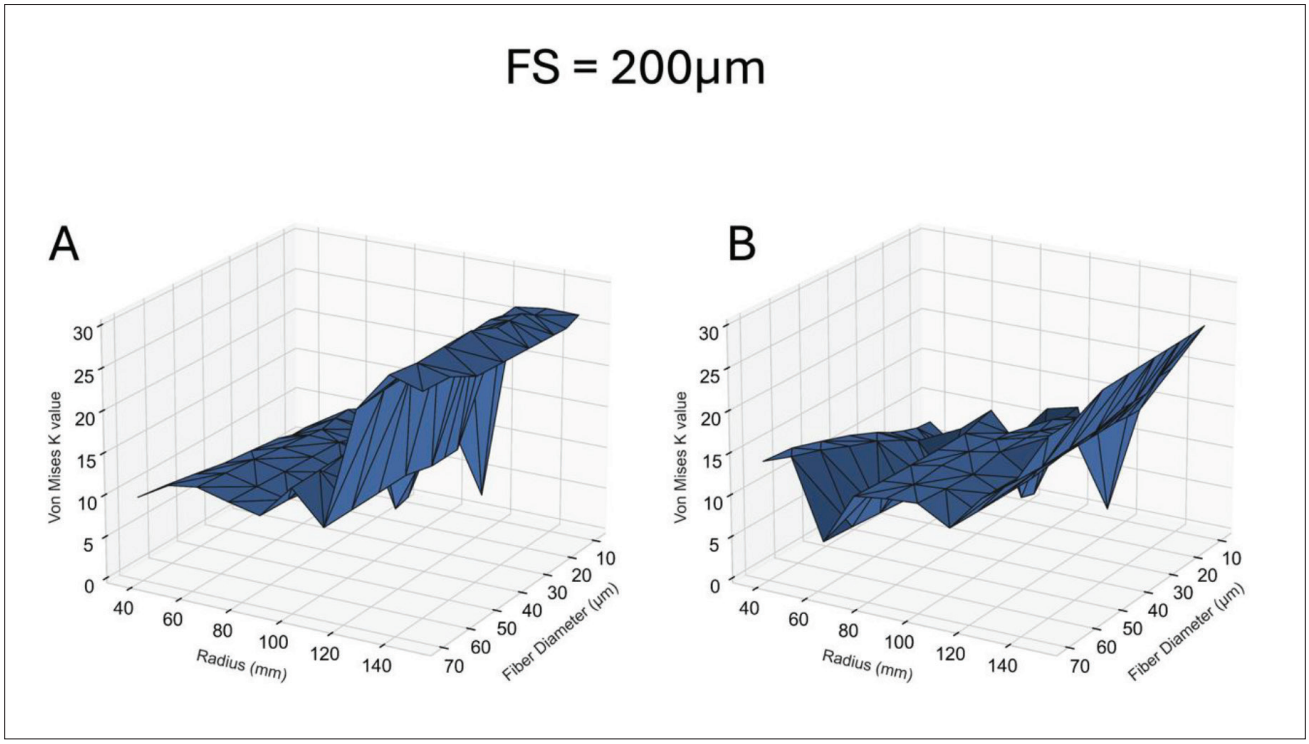

Figure S17. 3D plot of von Mises concentration coefficient (κ) and effects of scaffold parameters (radius [*R*] and fiber diameter [FD]) on κ for a single fiber spacing (FS) = 200 μm in the outer obtuse region (A) and middle obtuse region (B). Spearman's correlation coefficients for all *R*, FD, and FS input parameters were 0.86, −0.16, and −0.0073, respectively.

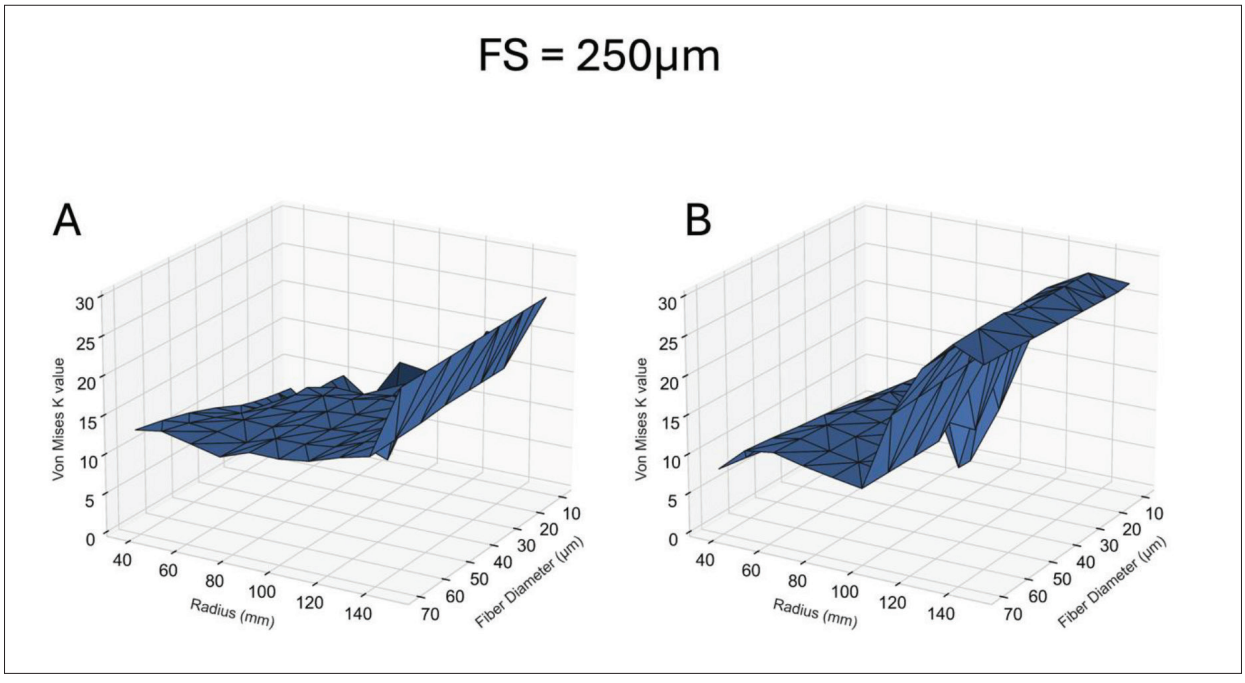

Figure S18. 3D plot of von Mises concentration coefficient (κ) and effects of scaffold parameters (radius [*R*] and fiber diameter [FD]) on κ for a single fiber spacing (FS) = 250 μm in the outer obtuse region (A) and middle obtuse region (B). Spearman's correlation coefficients for all *R*, FD, and FS input parameters were 0.86, −0.16, and −0.0073, respectively.

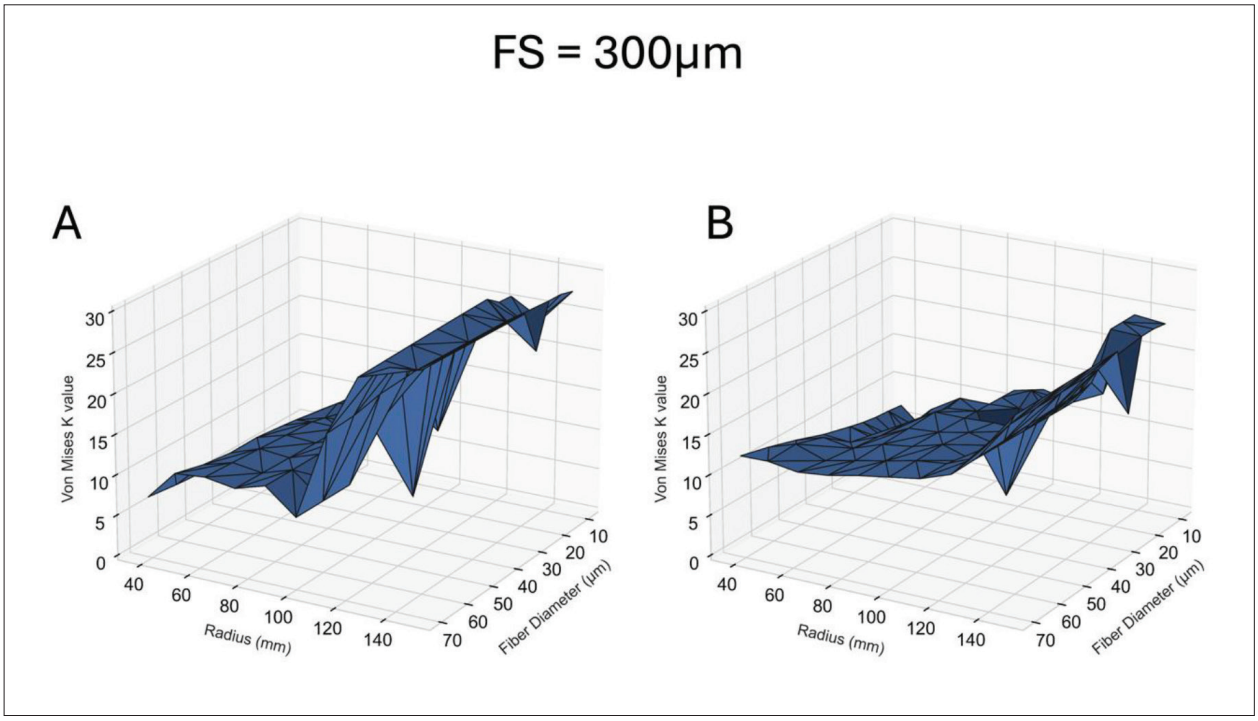

Figure S19. 3D plot of von Mises concentration coefficient (κ) and effects of scaffold parameters (radius [R] and fiber diameter [FD]) on κ for a single fiber spacing (FS) = 300 μm in the outer obtuse region (A) and middle obtuse region (B). Spearman's correlation coefficients for all R, FD, and FS input parameters were 0.86, −0.16, and −0.0073, respectively.

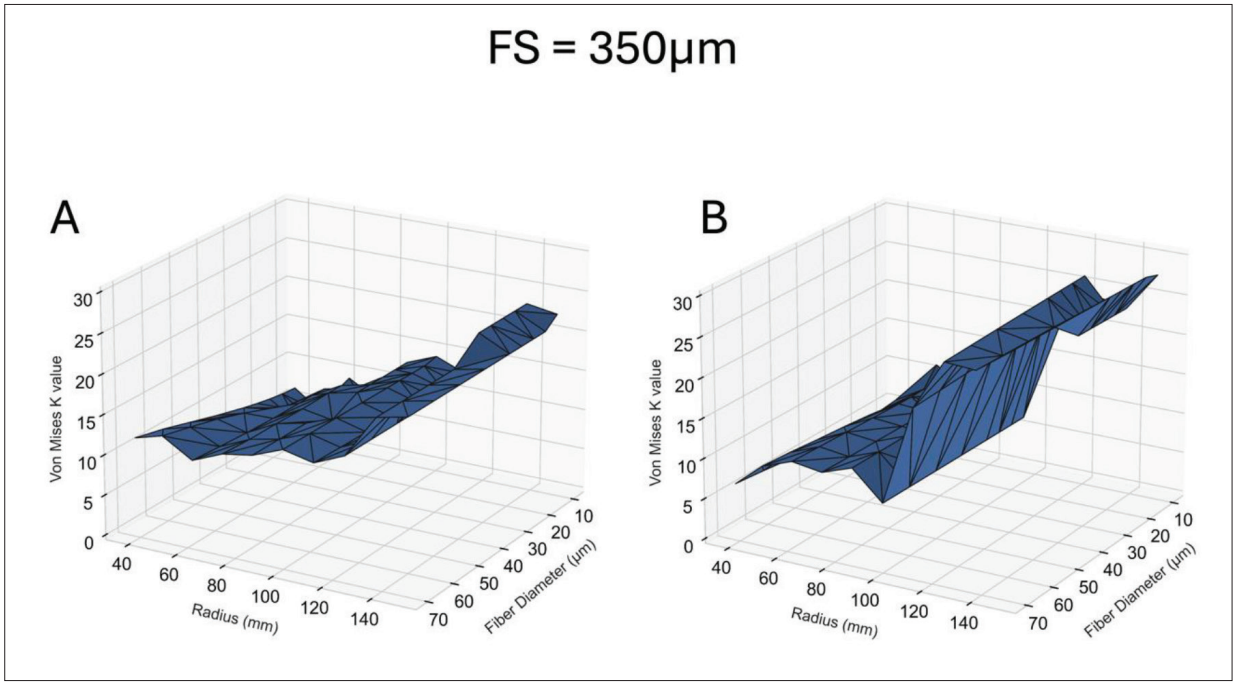

Figure S20. 3D plot of von Mises concentration coefficient (κ) and effects of scaffold parameters (radius [*R*] and fiber diameter [FD]) on κ for a single fiber spacing (FS) = 350 μm in the outer obtuse region (A) and middle obtuse region (B). Spearman's correlation coefficients for all *R*, FD, and FS input parameters were 0.86, −0.16, and −0.0073, respectively.

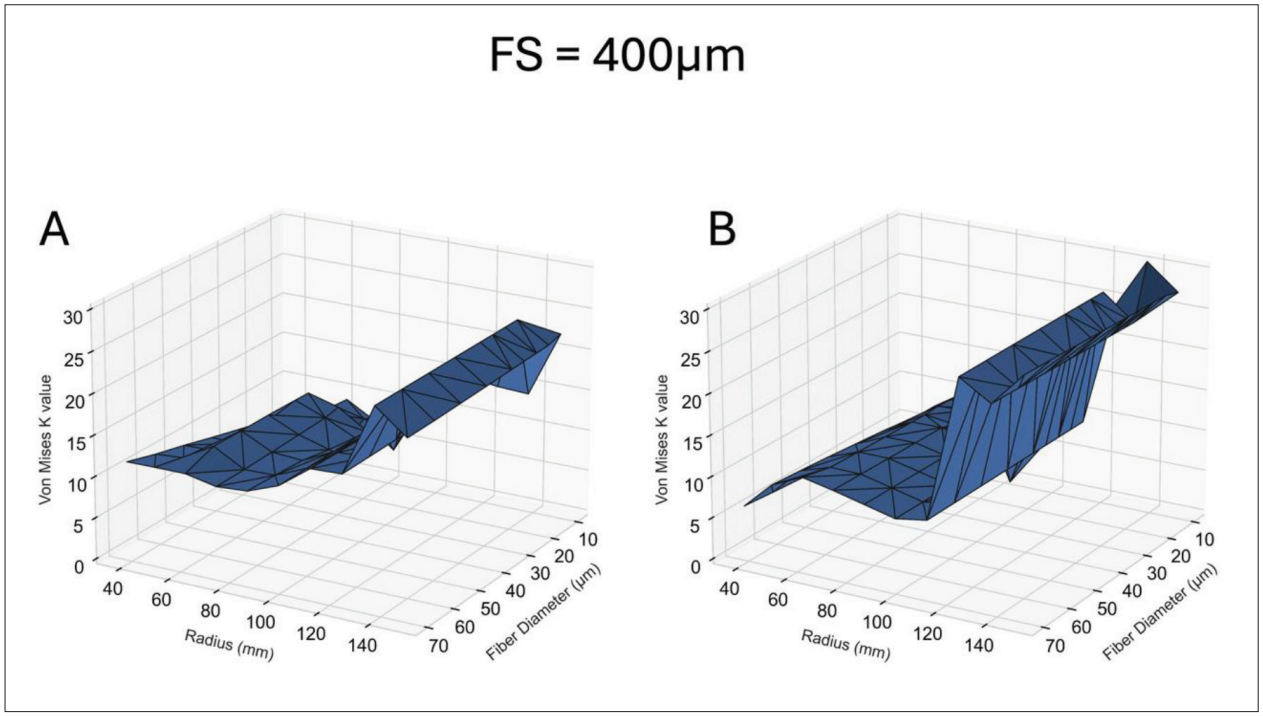

Figure S21. 3D plot of von Mises concentration coefficient (κ) and effects of scaffold parameters (radius [*R*] and fiber diameter [FD]) on κ for a single fiber spacing (FS) = 400 μm in the outer obtuse region (A) and middle obtuse region (B). Spearman's correlation coefficients for all *R*, FD, and FS input parameters were 0.86, −0.16, and −0.0073, respectively.

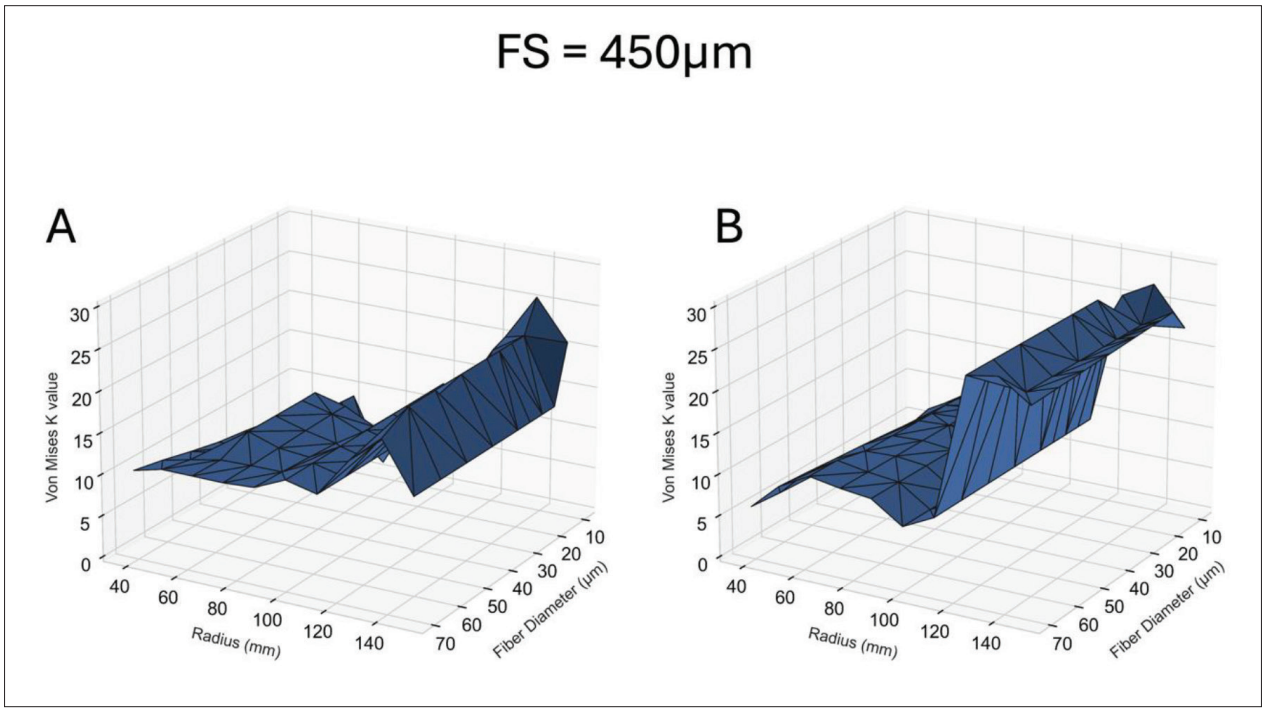

Figure S22. 3D plot of von Mises concentration coefficient (κ) and effects of scaffold parameters (radius [*R*] and fiber diameter [FD]) on κ for a single fiber spacing (FS) = 450 μm in the outer obtuse region (A) and middle obtuse region (B). Spearman's correlation coefficients for all *R*, FD, and FS input parameters were 0.86, −0.16, and −0.0073, respectively.

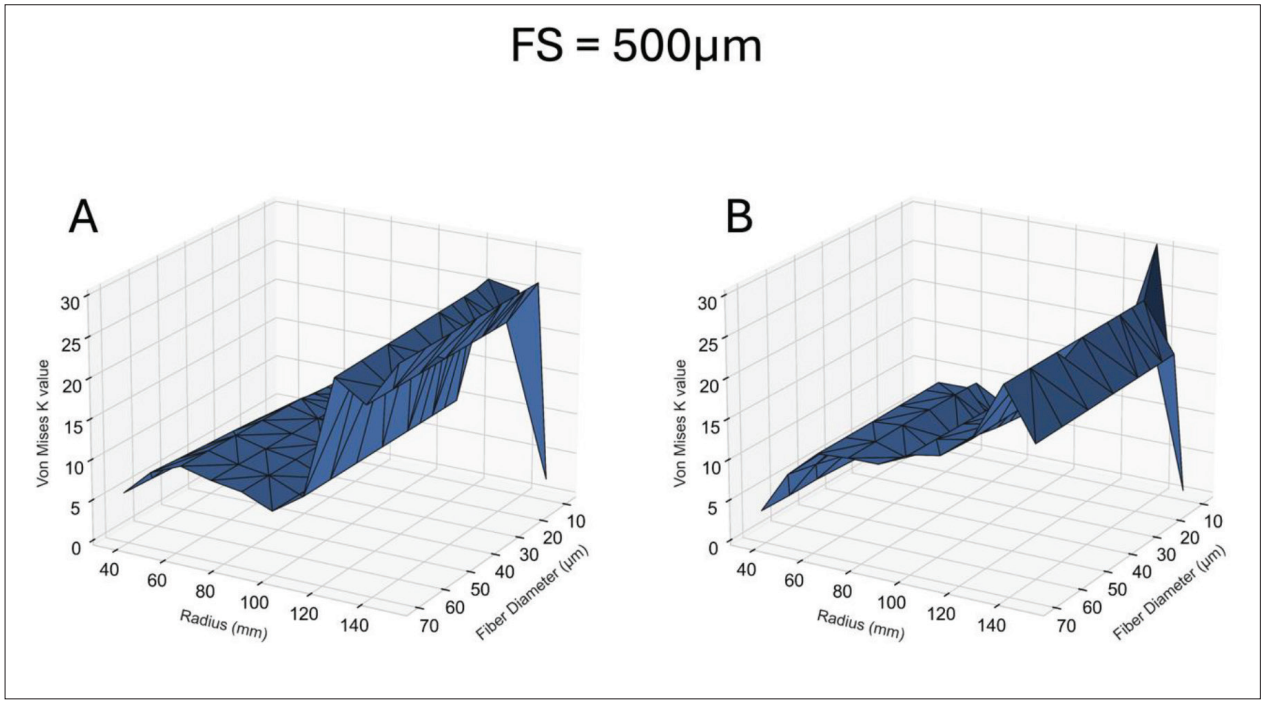

Figure S23. 3D plot of von Mises concentration coefficient (κ) and effects of scaffold parameters (radius [*R*] and fiber diameter [FD]) on κ for a single fiber spacing (FS) = 500 μm in the outer obtuse region (A) and middle obtuse region (B). Spearman's correlation coefficients for all *R*, FD, and FS input parameters were 0.86, −0.16, and −0.0073, respectively.

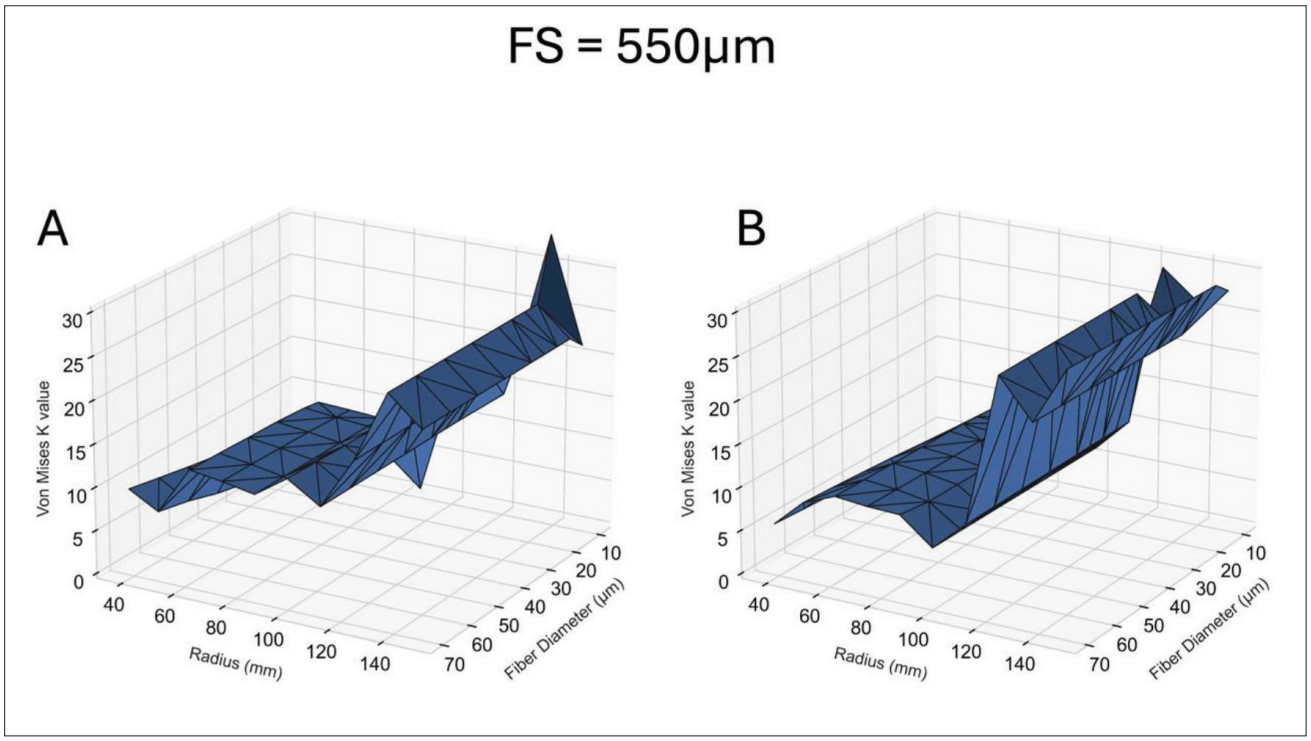

Figure S24. 3D plot of von Mises concentration coefficient (κ) and effects of scaffold parameters (radius [*R*] and fiber diameter [FD]) on κ for a single fiber spacing (FS) = 550 μm in the outer obtuse region (A) and middle obtuse region (B). Spearman's correlation coefficients for all *R*, FD, and FS input parameters were 0.86, −0.16, and −0.0073, respectively.